Nano-twines to twine-bridges: Role of force exerting perpendicular lateral protrusions in fibroblastic cell contraction

Authors:

Abinash Padhi[1], Karanpreet Singh[2], Janusz Franco-Barraza[3], Daniel J. Marston[4], Klaus M. Hahn[4], Edna Cukierman[3], Rakesh K. Kapania[2], and Amrinder S. Nain[1 *]

[1] Department of Mechanical Engineering, Virginia Tech, Blacksburg, Virginia, USA

[2] Department of Aerospace and Ocean Engineering, Virginia Tech, Blacksburg, Virginia, USA

[3] Cancer Biology Program, Marvin & Concetta Greenberg Pancreatic Cancer Institute, Fox Chase Cancer Center, USA

[4] Department of Pharmacology, The University of North Carolina at Chapel Hill, Chapel Hill, NC 27599

* Corresponding Author: nain@vt.edu

Keywords: Lateral protrusions, protrusive forces, anisotropic migration, aligned fibers, cell forces, cell protrusions, desmoplasia

ABSTRACT

Aligned fibrous matrices cause cells to have elongated shapes and anisotropic migration. Current research points to the maintenance of elongated cell shape due to reduced formation and activity of lateral protrusions. Here, we identify a new role of lateral protrusions that can originate from anywhere along the length of elongated cells and can apply contractile forces. Using aligned fiber networks that also serve as force sensors, we quantitate the role of lateral nano-projections (twines) that mature into broad perpendicular lateral protrusions (PLPs) through the formation of twine-bridges, thus allowing anisotropic cells to spread laterally. Using quantitative microscopy at the high spatiotemporal resolution, we show that twines of varying lengths can originate from stratification of cyclic actin waves traversing along the entire length of the cell, and not just at the leading edge. Primary twines can swing freely in 3D and engage with neighboring fibers in interaction times of seconds. Once engaged, the actin lamellum grows along the length of primary twine and re-stratifies to form a secondary twine. Engagement of secondary twine with the neighboring fiber leads to the formation of a suspended primary-secondary twine-bridge; a critical step in providing a conduit for actin to advance along and populate (mature) the twine-bridge. Using force vectors that originate from adhesion sites and directed along f-actin stress fibers, we quantitate the forces exerted by PLPs and find that the majority of force exerting PLPs are oriented perpendicular to the parent cell body. Our data highlights that cell spreading onto multiple fibers occurs through the engagement of PLPs with neighboring fibers and not necessarily from the leading edge. As cells spread on multiple fibers, they achieve higher contractility resulting in lower migration rates. Our identification of force exertion by PLPs that cause the fibers to bend inwards identifies desmoplastic expansion of the native extracellular matrix at single-cell resolution, thus providing new intervention opportunities in pathological biology.

INTRODUCTION

Cell migration is pivotal to many physiological and pathological processes[1], such as morphogenesis[2], wound healing[3] and tumor metastasis[4]. Cell migration is a complex process with cells often displaying plasticity in migratory modes, owing to the arrangement (dense vs. sparse or isotropic vs. anisotropic) and properties of surrounding extracellular matrix (ECM)[5–7]. Anisotropic migration utilizing multiple fibers simultaneously is of particular significance in the context of cancer metastasis[8,9] and wound healing[10]. During acute wound healing, myofibroblastic activation of local and/or recruited fibroblastic cells is required to impart inward forces and contract the collagen rich extracellular matrix (ECM) that, upon wound resolution, comprises the acellular scar. Similarly in solid epithelial tumors, like pancreatic ductal adenocarcinoma (PDAC), this chronic stroma reaction is known as desmoplasia[11]. Myofibroblastic cancer associated fibroblasts or myCAFs, are the local force-dependent activated cells responsible for the production and remodeling of the topographically aligned, anisotropic, desmoplastic ECM. To-date, the role of aligned ECM environments is implicated in inducing polarized migration, while very little is known on how and when desmoplastic expansion occurs and is maitained during disease onset and progression. It is commonly understood that in aligned ECM environments, cell polarity is maintained due to minimal probing in lateral directions.[12] In such scenarios, how cells stretch on multiple-fibers and whether spreading is driven primarily by leading edge probing, or through the formation of force exerting lateral protrusions along the cell body which aid in desmoplastic remodeling remain poorly described.

Lateral protrusions or spikes are well-documented in multiple cell types (growth cones, mesenchymal, fibrosarcoma, hepatocytes, and conjunctival cells)[13,14] in varying sizes (2-10 μm in length and 0.2-0.5 μm diameter).[14,15] They are implicated in the proteolytic degradation of the 3D interstitial ECM by cancer cells[14], and by leukocytes in probing the vascular membrane for permissive sites which eventually allows emigration into extravascular tissue[16]. In the case of leukocytes in the presence of shear flow, cells exhibit rolling via tethering by the formation of transient receptor-ligand bonds.[17,18] These are facilitated by microvilli shown to be 80nm in diameter and varying in length from 350 nm to 1 μm or longer[19,20]. Similarly, lateral protrusions formed in melanoma cells have also been documented to provide traction in a 3D environment in the absence of adhesion.[21] It was recently shown that spindle-shaped cells in 3D gel matrices form fewer lateral protrusions,[22] which is attributed to restriction in α5β1 integrin recycling to protrusions at leading edge [12,23], and or RhoA activation away from the leading edge which inhibits Rac1 thereby preventing the formation of lateral protrusions, thus helping maintain cell polarity and directed migration.[23–25] Overall, the utility of lateral protrusions remains partially understood as current cell culturing methods of 2D flat substrates limit the formation of lateral protrusions, and 3D gels lack the homogeneity to study them in a reproducible and replicable manner.

Using fiber diameters of curvature contrast, we have recently shown the ability to study lateral protrusions of various shapes and sizes formed in an integrin-dependent manner on fibers of different diameters.[26] Here, using aligned and suspended fiber nanonets that also act as force sensors, we report that anisotropically stretched cells (of different lineages) can form lateral protrusions that can swing freely in 3D (integrin-independent) and can attach to neighboring fibers in an integrin-adhesion manner in a matter of seconds. The filamentous lateral protrusions (primary filopodial *twines*) originating from the stratification of actin waves act as catalysts for the formation of *secondary twines*. We show that suspended *twine-bridges* composed of primary-secondary twines oriented perpendicular to cell body mature into lamellipodial resembling structures (perpendicular lateral protrusions (PLPs)) capable of exerting forces, thus allowing the anisotropically stretched cells to spread in the transverse direction, which ultimately increases the overall cell contractility and a decrease in migration speed. Altogether, our findings quantitatively describe the utility of lateral protrusions in anisotropic single cell migration.

RESULTS and DISCUSSIONS

Twines emerge from actin lamellum and engage neighboring fiber in seconds

We inquired if lateral protrusions could be formed in anisotropically stretched cells in an integrin-free manner, and used the previously described non-electrospinning (Spinneret based Tunable Engineered Parameters, STEP[27–29]) method to fabricate aligned fibers that also served as force sensing nanonets.[30,31] We observed the immortalized mouse (myoblast C2C12, embryonic fibroblast (MEF), and fibroblast NIH 3T3) and human Hela cell lines to migrate anisotropically in elongated shapes and form lateral protrusions (shown by yellow arrows in **Figure 1A**, and Movies 1-4). We then inquired if this behavior was conserved across primary cell lines and chose human mesenchymal stem cells (hMSCs) known for their migratory and differentiation potential. Due to the large size of hMSCs, they were found to attach to at least three fibers (for the fiber spacing of scaffolds used in this study) (**Figure 1B**). Cells continuously formed nano-filamentous structures, termed *twines* (shown by yellow arrows in Figure 1B) lateral to the polarized direction of the cell. The *twines* were observed to attach to neighboring fibers, become thicker (mature) and apply contractile forces evidenced by deflection of neighboring fiber (Movie 5). We found that *twines* originated from membrane ruffles that resembled previously described cyclic actin waves[32]. The membrane ruffles spiraled about the fiber axis (**Figure 1C** and Movie 6) as they advanced at 6.58 µm/min (n=30)

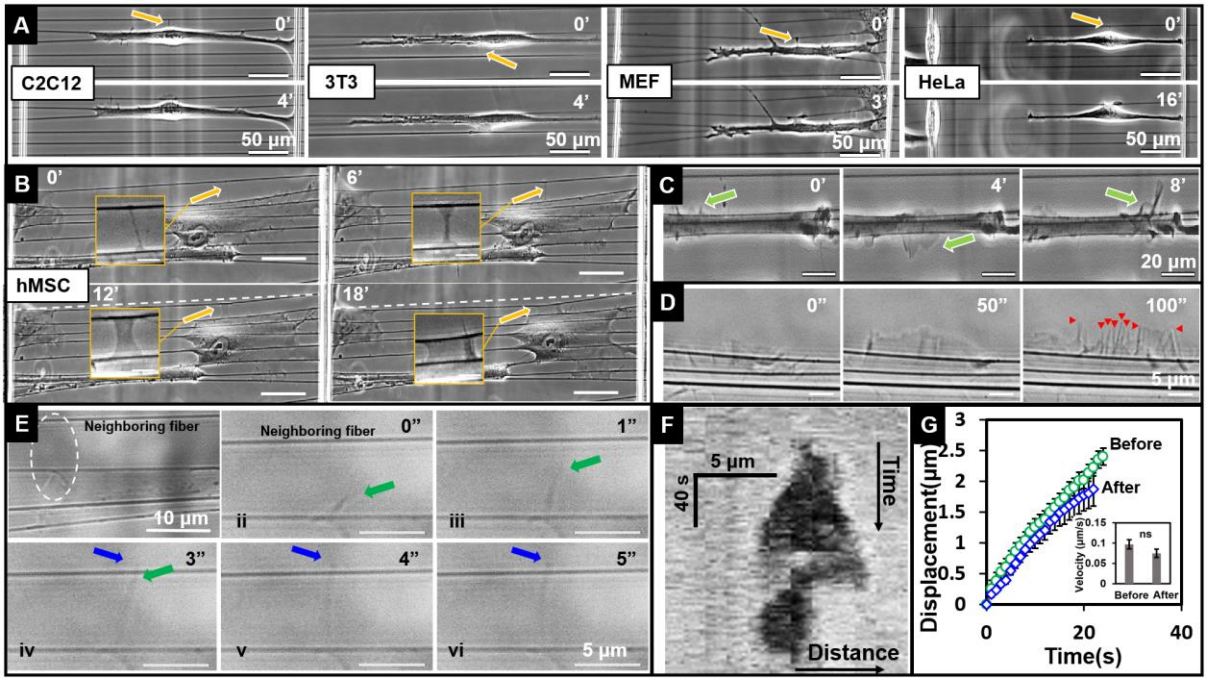

FIGURE 1. Lateral protrusions in anisotropically stretched cells and kinetics of *twine* formation. Time-lapse images showing (A) thin filopodial lateral protrusions (shown by arrows and termed *twines*) formed away from the leading edge mature into broad lamellipodial structures in four different cell types stretched anisotropically on aligned and suspended fibers (Movies 1-4), (B) growth of twine (pointed by arrow) from filopodial to lamellipodial structures in human mesenchymal stem cell (hMSC, Movie 5). Insets shows magnified images with scale bar 10 µm. (C) Actin wave (green arrow) travelling along the length of cell body (Movie 6). (D) Actin wave ruffles develop into striated structures leading to formation of nano-filamentous '*twines*' shown by red arrowheads (Movie 7). (E) i. Image of a cell with *twine* shown by yellow arrow. (ii-vi) Time-lapse images of area indicated by dashed oval demonstrating that *twine* engagement with neighboring fiber takes place in ~seconds (Movie 8). Green arrow shows growth of *twine* from cell body and blue arrow shows *twine* growth after engagement with neighboring fiber i.e. overhanging part of *twine*. (F) Kymograph obtained by performing line scan along the fiber axis demonstrating increase in *twine* width on neighboring fiber post engagement. (G) The average displacement vs. time profiles of advancement of *twine* before and after engagement with neighboring fiber (n=17 for both). Inset shows average velocity for the two categories.

similar to actin polymerization rates reported in the literature (7.20-8.73 μm/min).[33] The ruffles extended beyond the main cell body and stratified into denser independent structures (*twines*, **Figure 1D** and Movie 7) presumably due to folding-over and buckling.[34] The *twines* were found to grow in length at the rate of ~0.1 μm/s, and swing freely (3D) in the media similar to reported angular rotations of filopodia,[35–38] which allowed them to engage (attach) to a neighboring fiber. The attachment to neighboring fiber occurred in a matter of seconds (**Figure 1E, F** and Movie 8), and post engagement the *twines* continued to grow at rates similar to pre-engagement (inset in **Figure 1G**). Our observation of *twine-fiber* interactions occurring over seconds is in agreement with a recent study showing fibroblasts adhering to fibronectin in ≤ 5s by utilizing α5β1 integrin's.[39] Physically, the *twines* resemble microspikes and filopodia that are reported to exceed lengths of ~10 μm rarely,[40] whereas the lengths of *twine*s observed by us had a wide distribution (short ~ 5 μm to extremely long ~ 35 μm). To the best of our knowledge, filopodia of similar or longer lengths have been reported only in the case of sea urchin embryos.[41] Unlike the location of origin of filopodia, *twines* formed from stratified actin-membrane ruffles originate laterally along the entire length of the cell body, and their growth rate (~0.1 μm/s) match the reported kinetics of filopodia (extension rate ~0.12-0.2 μm/s[42]), thus suggesting actin to be the main constituent of *twines*.

Twine-bridges used in cell spreading

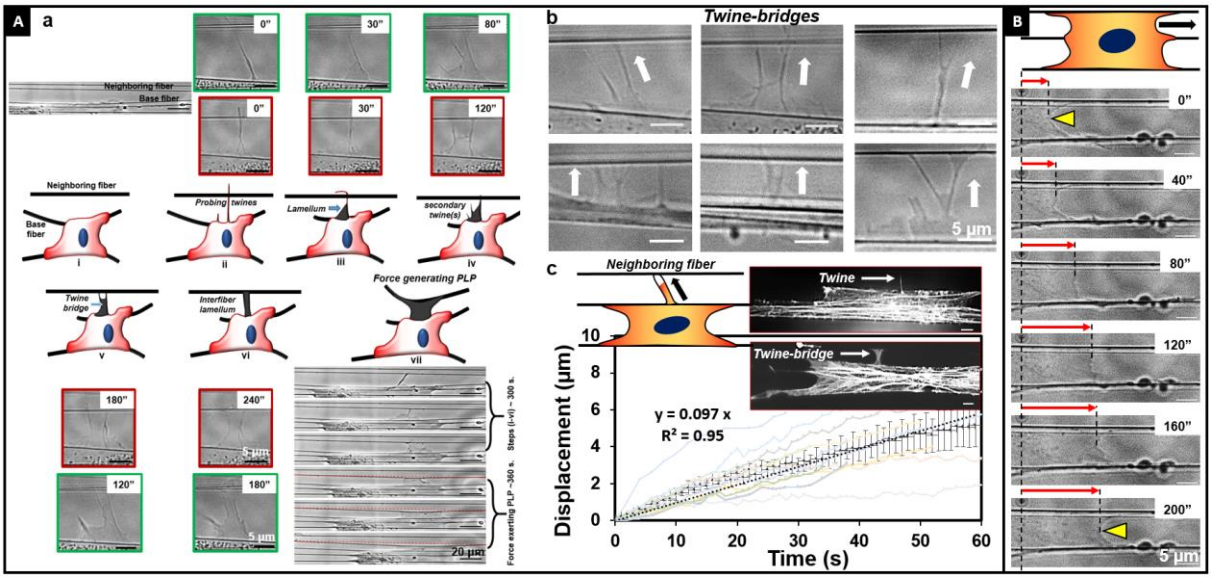

FIGURE 2. *Twine-bridges.* (A) a) Cartoons showing the process of forming force exerting perpendicular lateral protrusions (PLPs). Cells attached to fibers form filamentous *twines* that engage with with neighboring fiber (i). Subsequently, actin lamellum grows along the base of *twine* from cell body (ii) followed by s formation of secondary *twines* (iii). Engagement of secondary *twine* with neighboring fiber leads to formation of a suspended primary-secondary *twine-bridge* (iv) that facilitates advancement of actin that generates a suspended *interfiber lamellum* (v). Over time (~minutes), the interfiber lamellum broadens and applies contractile forces causing neighboring fiber to bend, thus creating force exerting PLPs(vii). Phase images in in green and red boxes depict two sample cases of PLPs in steps (i-vi), and phase images of whole cell (top left) forming PLP is shown (bottom right). Red dashed lines indicate undeflected position of neighboring fiber b) Sample images of *twine-bridges* of varying sizes and shapes and arrows point to *twine-bridge* development towards the neighboring fiber. c) Displacement vs. time profiles showing extension rates of actin lamellum between *twine-bridges* (n=13). Inset shows cartoon of actin lamellum advancement along the *twine-bridge* and images of a single *twine* and *twine-bridge* obtained by fixed staining for f-actin in two separate cells with scale bar 10 μm. (B) Time-lapse images of actin membrane advancement of cell attached to parallel fibers showing the similarity in actin advancement observed in *twine-bridges*. Yellow arrows show the concave edge of cell between fibers before and after actin membrane advancement.

Next, we inquired how *twine* structures matured (became thicker). Usage of 63X magnification and 1 s imaging allowed us to identify and quantitate formation of secondary *twines* and *twine-bridges* (Movie 9). As described before, the thin nano-filamentous primary *twine* (**Figure 2A**) that emerged lateral to the cell body first engaged with a neighboring fiber. The fixed attachment of the *twine* to the fiber can be inferred from the changing direction of overhanging growth of primary *twine* (Figure 1D, time point 4 and 5 seconds shown by the blue arrow). Once engaged, we observed the emergence and growth of actin lamellum at the base of the primary *twine* (Figure 2A a(iii)). Similar to folding and buckling driven stratification of membrane ruffle described before (Figure 1C), we observed the formation of *secondary twines* (Fig. 2A a(iv)) from the actin lamellum. Engagement of the secondary twine with the neighboring fiber resulted in the formation of a suspended primary-secondary *twine-bridge* (Figure 2A a(v)) of different shapes (**Figure 2A b**) that facilitated actin lamellum advancement at the rate of ~0.1 μm/s (**Figure 2A c**), similar to actin polymerization rates (~0.12-0.14 μm/s)[33] but faster than actin retrograde flow rates (~0.008-0.025 μm/s in the lamellipodial tip or ~0.004-0.008 μm/s in the lamella).[43] Filopodia-lamellipodia transitions previously studied on 2D flat substrates depend upon the available integrin adhesion sites along individual filopodia at the leading edge, and occur either through veil advancement in neuronal growth cones[44] or from broadening of the filopodia.[45] Contrastingly, we show that *twine-bridge* maturation that resembles filopodia-lamellipodia transitions (PLPs) is integrin-independent along the length of *twine-bridge*, and occurs at any location along the cell body through actin lamellum advancement. We also inquired if actin membrane advancement was conserved at a larger scale of single cells attached between fibers and if the fibers themselves acted as *bridges*. Interestingly, we found that actin membrane advancement between fibers (**Figure 2B**) initiated after a break in the concave symmetric outline of cell body followed by rapid advancement of actin membrane (~0.07 μm/s, Supplementary Fig. S1) that culminated with re-establishment of concave symmetric cell shape (shown by yellow triangles). Altogether, our findings demonstrate that bridges (*twine* and fibers) formed between at least two aligned twines or two fibers respectively, promote the advancement of actin lamellum at multiple length scales.

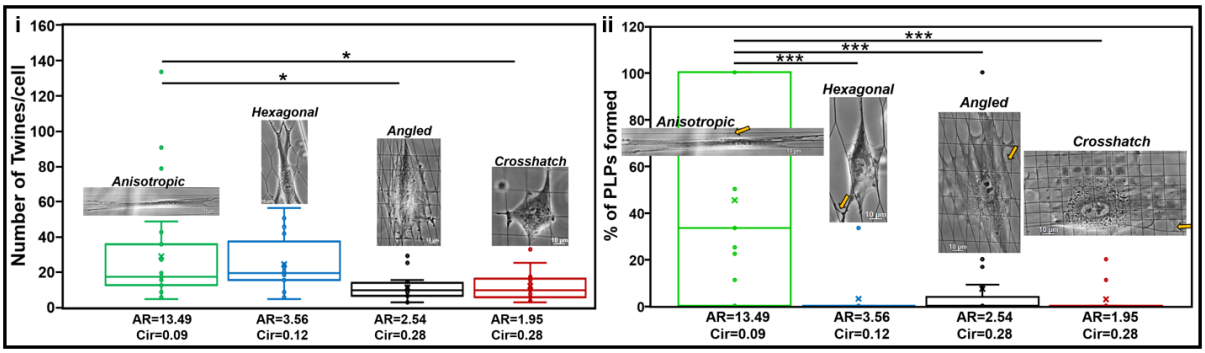

FIGURE 3. *Twine and PLP events.* Four fiber network designs were created to interrogate cell shape (AR: aspect ratio and Circ.: circularity) driven number density of (i) *twines,* and (ii) *PLP* formation ((number of PLPs/number of attached twines)*100).

Next, we inquired if the observed behavior of *twines* and PLPs were exclusive to cells attached to parallel fiber networks. We constructed three more designs (hexagonal, angled and crosshatches) and recorded the number of *twines* (length ≥ 3 μm) forming in cells on each fiber category, with the highest number of *twine* formation per cell over a two-hour period (imaged every two minutes) occurred in cells with high aspect ratios (parallel and hexagonal, **Figure 3(i)**). Since *twines* were attaching to neighboring fibers in all categories, next, we calculated the number of PLPs formed from these attached *twines* (**Figure 3(ii)**). Not surprisingly, we found that on average nearly half of engaged *twines* transitioned to a PLP in cells attached to anisotropic parallel fibers, whereas for all other fiber networks, we rarely encountered formation of PLPs. Altogether, our data suggest that elongated cells (high aspect ratio and low circularity) promote maximum formation of *twines*, and only parallel arrangement of fibers (not the cell shape) promote

transitioning of attached *twines* to PLPs. We note that in our analysis, we have excluded cases of dense parallel networks of low interfiber spacing that do not display the transition of *twine* to PLP (**Figure 2a**). In these cases, either the ruffles directly attach to the neighboring fiber or thicker twines that attach to neighboring fibers do not display all the steps outlined in Figure 2a (Movies 10 and 11).

Forces of *twine-bridges*

It is now well appreciated that cells in *in vivo* and in 3D interstitial ECM exert contractile forces on the neighboring fibrous environments either by pushing or tugging at individual fibers.[14,46,47] In a similar manner, we also observed that *twines* that transitioned to broad lamellipodial resembling structures were able to pull neighboring fibers inwards towards the cell body, thus allowing the cells to spread on multiple fibers. Thus, we inquired the development of forces in PLPs and consequential migratory and force response of cells as they spread from three to four and five fibers.

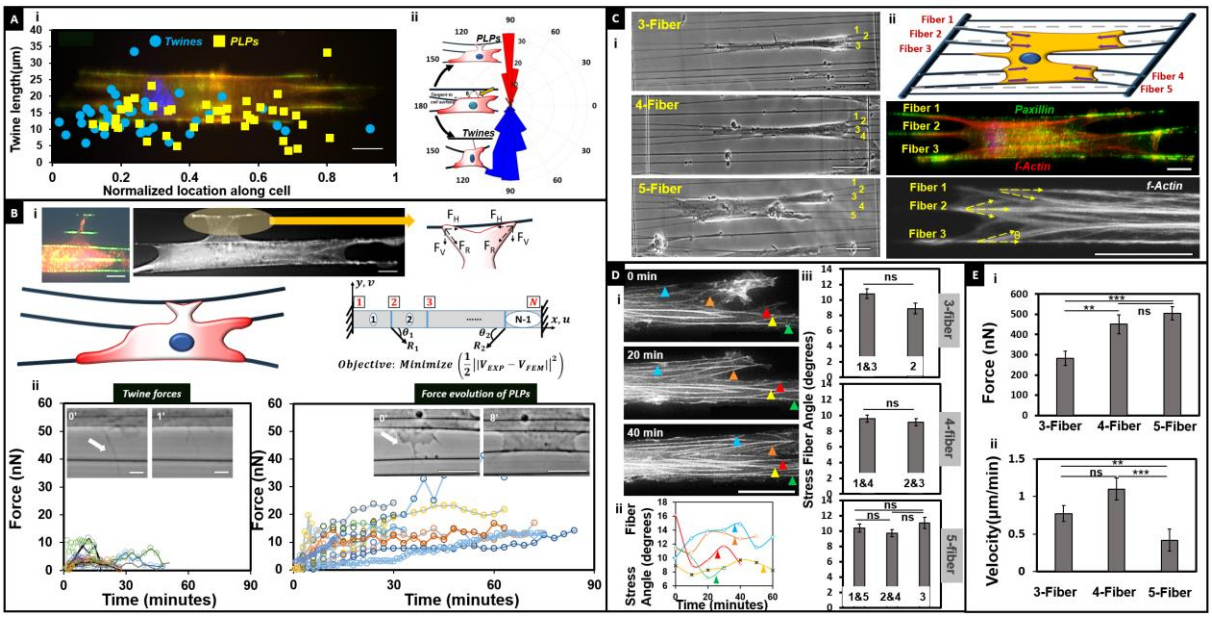

FIGURE 4. **Forces applied by *twine-bridges* facilitate cell spreading**. (A) i. Plot showing the length of *twines* observed with respect to corresponding location of emergence of *twines* and PLPs along the normalized cell length. Actin is denoted by red, paxillin by green and nucleus by blue. ii. Polar histogram of initial *twine* engagement angles with neighboring fiber for PLP and *twine* cases (n=84 for PLP and 123 for *twines*). PLPs are mostly perpendicular to cell body. (B) i. Representative *twine-bridges* (scale bar 10 μm) along with representation of forces exerted by developing *twine-bridge*. Force vectors are assumed to act along the membrane curvature with origin at paxillin cluster lengths (green). To evaluate the forces, the deflected fiber is modelled as beam with fixed-fixed boundary condition. The force vectors R_1 and R_2 are calculated by minimizing the objective function, where V_{EXP} represents the displacement profile of the beam measured from image sequences and V_{FEM} is the prediction from finite element model (see Supplementary information for details on model). ii. Force response of *twine-bridges* over time for undeveloped and developed category with inset images showing both categories. Developing *twine-bridges* allow cells to spread across multiple fibers. (C) i. Representative phase images of anisotropically stretched cells on 3, 4 and 5 fibers. ii. Schematic representation of NFM method to measure contractile forces of single cells attached to multiple fibers. The direction of force vectors are determined from paxillin focal adhesion clustering (FAC shown by green) acting along f-actin stress fibers (red and white). (D) i. Time-lapse images showing stress fibers tracked for angular measurements in a cell attached to five fibers. ii. Triangles of different colors in fluorescent image correspond to the transient plot. Measurements of all stress fibers could not be taken for the entire one-hour period as the respective cell front migrated out of the field of view. iii. The average f-actin stress fiber angle data: 3-fiber category: fiber 1&3 (n=53, n signifying number of stress fibers), fiber 2 (n=30). 4-fiber category: fiber 1&4 (n=80), fiber 2&3 (n=84). 5-fiber category: fiber 1&5 (n=72), fiber 2&4 (n=70), fiber 3 (n=35). (E) i. Average of total force calculated for 3 time points separated by 3 minutes each for spread cells selected randomly (n=13, 14 & 15 for 3, 4 & 5 fiber categories respectively). ii. Average migration rates for each fiber category (n=15 in each). Scale bar is (A) 20μm, (C)i. 50μm and ii. 20μm, (D)i. 20 μm.

First, we recorded that *twines* and PLPs of varying lengths (5-35 µm) formed along the entire length of the cell body (**Figure 4A i**) and in certain instances were able to deflect the neighboring fibers to which they had attached. We classified the ability of these structures to exert force if they deflected the neighboring fibers ≥2 µm. Intriguingly, we found that while *twines* attached to neighboring fibers over a wide range of angles, the ensuing PLPs were recorded to be to be primarily oriented orthogonal to the parent cell body (**Figure 4A ii**). Next, we quantitated the forces exerted by both *twines* and PLPs using Nanonet Force Microscopy (NFM[30,31], **Figure 4B i**) that calculates the forces through the establishment of *realistic* tension bearing force vectors directed towards the cell body. Specifically, the vectors originate at the paxillin attachment points and are pointed along the dominant stress fibers defining the membrane curvature. A single force vector was assigned for PLP less than six µm in width, and two force vectors on either side of PLP were assigned for sizes greater than six µm. Our analysis that minimizes the difference between experimental data (measured fiber displacement profile) and finite element model prediction revealed that *twines* angled from the parent cell body could apply forces for only a brief period which prevented their maturation into broad lamellipodial PLP structures (**Figure 4B ii**). Interestingly, we found that twines that were angled to parent cell body transitioned to PLPs as the cell body moved thus changing the angle of attachement (Movie 12). While individual filopodia have been shown in the past to exert forces (~2nN)[48], here using NFM we quantitate the transient force response of *twines* from thin to thick lamellipodial resembling structures capable of exerting higher forces (tens of nanonewton), thus providing the necessary support for cells to spread onto neighboring fibers. In contrast to other methods where the force vectors are determined independent of stress fiber orientation,[49–51] our method integrates arrangement of adhesion sites that are unique to cells attached to ECM mimicking fibers,[30] with actin cytoskeleton contractility.

Next, since cells were using *PLPs* in anisotropic cell migration to spread onto neighboring fibers, we inquired how the *inside-out* contractile state of cells changed when they spread from 3 to 4 and 5 fibers (**Figure 4C i**). For the calculation of forces applied by cells, we approximated a strategy of using a single force vector that originated at the site of paxillin focal adhesion clustering (FAC) and pointed along the dominant f-actin stress fiber (**Figure 4C ii**). We chose this strategy based upon our previous finding that cells attached to ~250 nm diameter fibers by forming FAC at the poles and diffuse distribution of adhesions along the cell-fiber length.[30] We quantified the transient change in stress fiber angles as cells migrated and observed them to maintain their relative positions on all fiber categories (**Figure 4D i,ii**, Supplementary Fig. S2 and Movie 13). Overall, the stress fibers were found on average to be angled between 8-11 degrees on all fiber categories (**Figure 4D iii**). The overall contractile force was computed by summation of the individual forces acting at the adhesion clusters ($F_{Cell} = \sum F_{FAC}$). Cells spread on 5 fibers exerted higher forces (~505 nN), and as a consequence had statistically lower migration rates compared to those on 3 (~282 nN) or 4 fibers (~451 nN) (**Figure 4E**). We found that cells attached to fibers had a symmetric distribution of forces with the highest contractility driven by fibers at the outermost boundaries of cells (Supplementary Fig. S3).

CONCLUSIONS

In conclusion, using NFM, we show in a reproducible and replicable manner that anisotropically stretched cells of varying lineages can spread on multiple fibers in the lateral direction through the formation of lateral protrusions. Our findings identify a new category of lateral protrusions, and we show that elongated cells form highest number of lateral *twines,* and only parallel arrangement of fibers as observed in pathological fibrous environments promote the maturation of *twines* to force exerting perpendicular lateral protrusions (PLPs). We caution that our *in vitro* fibrous assay attempts to recapitulate the complex native environment in which few cell attachment points (large pore size) force cells to make contact with only single fibers. [5,52,53] Further improvements in density, organization, and size of fibers will provide a more comprehensive understanding of the role of lateral protrusions in cells attached to a multitude of fibers in both aligned (Movie 14) and random fibrous environments representing pathological and physiological environments respectively. Moving forward, the flexibility of our method and model complemented with live

microscopy of adhesion sites and stress fibers will allow us to describe the time variant load distributions at adhesion sites (FAC and along the cell body), along with cytoskeletal component orientations for a comprehensive description of force distribution in-line and lateral to the cell migration direction. In future, coupling the force response with live-imaging of RhoGTPase signaling in PLPs from any site on the cell body and linking it with the leading edge will provide a comprehensive description of the role of *PLPs* in the in pathological cancer biology.

METHODS

Nanonet Manufacturing and Cell Culture:

The suspended polystyrene fibers were manufactured by the previously reported non-electrospinning STEP technique.[28] A network of small diameter parallel fibers (~250 nm) was deposited 5-7 µm apart upon a layer of base fibers (~ 1 µm) spaced 350 µm apart and fused at the interjections. The scaffolds were placed in glass bottom 6-well plates (MatTek, Ashland, MA) and sterilized in 70% ethanol for 10 min. After two rounds of PBS (1x) wash, 50 µl of 4µg/ml of Fibronectin (Invitrogen, Carlsbad, CA) was put on the scaffolds and incubated at 37°C for 30 min to facilitate cell adhesion. Bone Marrow-derived human Mesenchymal Stem Cells, hMSCs (Lonza Inc, Basel, Switzerland) were cultured in supplemented growth medium (Lonza Inc) at 37°C and 5% CO2. Cells were seeded on the scaffolds by placing 50 µl droplets of 100,000 cells/mL on the suspended part, and 300 µl of media was placed around the well to prevent evaporation. After incubation for 2hr to facilitate attachment, two mL of supplemented growth medium was added to each well.

Time Lapse Microscopy and Cell Force Calculations

Nanonets in 6 well plate were placed in an incubating microscope (AxioObserver Z1, Carl Zeiss, Jena, Germany). Time Lapse movies were created by taking images at 20x at 3min or 40/63X at the 1-second interval with an AxioCam MRm camera (Carl Zeiss). All measurements were performed using AxioVision (Carl Zeiss) and ImageJ (National Institute of Health, Bethesda, MD). Using beam mechanics, cell forces were estimated from experimentally obtained deflection of fibers. Briefly, an optimization algorithm written in MATLAB (MathWorks, Natick, MA) matched the experimental and computational finite-element fiber deflections to calculate forces at each time point (for details on model development, optimization algorithm and validation tests see supplementary information).

Immunohistochemistry and Immunofluorescence Imaging

Cells on fibers were fixed in 4% paraformaldehyde, permeabilized in 0.1% Triton X100 solution and blocked in 5% goat serum. Paxillin staining was done using primary rabbit anti-paxillin antibodies (Invitrogen) at a dilution of 1:250 and incubated at 4°C for 1h. Secondary goat anti-rabbit Alex Fluor 488 (Invitrogen) antibodies were incubated for 45 min at room temperature in the dark. F-Actin stress fibers were stained using Rhodamine Phalloidin. Cell nuclei were stained with 300 nM of DAPI (Invitrogen) for 5 min. The scaffolds were kept hydrated in 2ml PBS (phosphate-buffered saline) during imaging. Fluorescent images were taken using an Axio Observer Z1 microscope (Carl Zeiss). Actin live cell imaging was performed as per manufacturer's instructions on using the reagent CellLight Actin-RFP, Bacman 2.0 (Invitrogen).

Statistical Analysis

Sample populations were tested for statistical significance using the Student's t-test and analysis of variance (ANOVA) for multiple group comparisons in GraphPad software (GraphPad Prism, California). Error bars represent standard errors. Values are reported as an average ± 1 SE. * denotes p-value ≤ 0.05, ** p-value ≤ 0.01, and *** denotes p-value ≤ 0.001.

ACKNOWLEDGMENTS

ASN, EC and KMH are thankful to late Professor Keely (University of Wisconsin) for discussions and guidance on cell biology and dedicate this manuscript in her remembrance. ASN would like to acknowledge the Institute of Critical Technologies and Sciences (ICTAS) at Virginia Tech for the support to conduct this study. AP and ASN would like to thank members of the STEP Lab for their helpful suggestions and discussions.

Declaration

The authors declare no competing interests.

Author Contributions

ASN, EC, and KMH designed the research. ASN supervised the research. AP performed the experiments and conducted the analysis. AP, DM and JF analyzed the IF images. KS and RKK developed the analytical and finite element model. AP, EC, KMH and ASN wrote the manuscript.

Funding Sources

This work is supported by National Science Foundation (NSF 1437101 and 1462916) awarded to ASN.

REFERENCES

(1) Lo, C. M.; Wang, H. B.; Dembo, M.; Wang, Y. L. Cell Movement Is Guided by the Rigidity of the Substrate. *Biophys. J.* **2000**, *79*, 144–152.

(2) Juliano, R. L.; Haskill, S. Signal Transduction from the Extracellular Matrix. *J. Cell Biol.* **1993**, *120*, 577–585.

(3) Martin, P. Wound Healing--Aiming for Perfect Skin Regeneration. *Science (80-.).* **1997**, *276*.

(4) Bernstein, L. R.; Liotta, L. A. Molecular Mediators of Interactions with Extracellular Matrix Components in Metastasis and Angiogenesis. *Current opinion in oncology*, 1994, *6*, 106–113.

(5) Friedl, P.; Wolf, K. Plasticity of Cell Migration: A Multiscale Tuning Model. *J. Cell Biol.* **2010**, *188*, 11–19.

(6) Petrie, R. J.; Yamada, K. M. Multiple Mechanisms of 3D Migration: The Origins of Plasticity. *Curr. Opin. Cell Biol.* **2016**, *42*, 7–12.

(7) McNiven, M. A. Breaking Away: Matrix Remodeling from the Leading Edge. *Trends Cell Biol.* **2013**, *23*, 16–21.

(8) Keikhosravi, A.; Bredfeldt, J. S.; Sagar, A. K.; Eliceiri, K. W. *Second-Harmonic Generation Imaging of Cancer*; 1st ed.; Elsevier Inc., 2014; Vol. 123.

(9) Provenzano, P. P.; Eliceiri, K. W.; Campbell, J. M.; Inman, D. R.; White, J. G.; Keely, P. J. Collagen Reorganization at the Tumor-Stromal Interface Facilitates Local Invasion. *BMC Med.* **2006**, *4*, 38.

(10) Petroll, W. M.; Cavanagh, H. D.; Barry, P.; Andrews, P.; Jester, J. V. Quantitative Analysis of Stress Fiber Orientation during Corneal Wound Contraction. *J. Cell Sci.* **1993**, *104 (Pt 2*, 353–363.

(11) Alexander, J.; Cukierman, E. Stromal Dynamic Reciprocity in Cancer: Intricacies of Fibroblastic-ECM Interactions. *Curr. Opin. Cell Biol.* **2016**, *42*, 80–93.

(12) Riching, K. M.; Cox, B. L.; Salick, M. R.; Pehlke, C.; Riching, A. S.; Ponik, S. M.; Bass, B. R.; Crone, W. C.; Jiang, Y.; Weaver, A. M.; *et al.* 3D Collagen Alignment Limits Protrusions to Enhance Breast Cancer Cell Persistence. *Biophys. J.* **2014**, *107*, 2546–2558.

(13) Adams, J. C. Cell-Matrix Contact Structures. *Cell. Mol. Life Sci.* **2001**, *58*, 371–392.

(14) Wolf, K.; Friedl, P. Mapping Proteolytic Cancer Cell-Extracellular Matrix Interfaces. *Clin. Exp. Metastasis* **2009**, *26*, 289–298.

(15) Taylor, A. C.; Robbins, E. Observations on Microextensions from the Surface of Isolated Vertebrate Cells. *Dev. Biol.* **1963**, *7*, 660–673.

(16) Nourshargh, S.; Hordijk, P. L.; Sixt, M. Breaching Multiple Barriers: Leukocyte Motility through Venular Walls and the Interstitium. *Nat. Rev. Mol. Cell Biol.* **2010**, *11*, 366–378.

(17) McEver, R. P.; Zhu, C. Rolling Cell Adhesion. *Annu. Rev. Cell Dev. Biol.* **2010**, *26*, 363–396.

(18) Ramachandran, V.; Yago, T.; Epperson, T. K.; Kobzdej, M. M.; Nollert, M. U.; Cummings, R. D.; Zhu, C.; McEver, R. P. Dimerization of a Selectin and Its Ligand Stabilizes Cell Rolling and Enhances Tether Strength in Shear Flow. *Proc. Natl. Acad. Sci. U. S. A.* **2001**, *98*, 10166–10171.

(19) Bruehl, R. E.; Springer, T. A.; Bainton, D. F. Quantitation of L-Selectin Distribution on Human Leukocyte Microvilli by Immunogold Labeling and Electron Microscopy. *J. Histochem. Cytochem.* **1996**, *44*, 835–844.

(20) Karnik, R.; Hong, S.; Zhang, H.; Mei, Y.; Anderson, D. G.; Karp, J. M.; Langer, R. Nanomechanical Control of Cell Rolling in Two Dimensions through Surface Patterning of Receptors. *Nano Lett.* **2008**, *8*, 1153–1158.

(21) Tozluoğlu, M.; Tournier, A. L.; Jenkins, R. P.; Hooper, S.; Bates, P. A.; Sahai, E. Matrix Geometry Determines Optimal Cancer Cell Migration Strategy and Modulates Response to Interventions. *Nat. Cell Biol.* **2013**, *15*, 751–762.

(22) Nelson, C. M.; Bissell, M. J. Of Extracellular Matrix, Scaffolds, and Signaling: Tissue Architecture Regulates Development, Homeostasis, and Cancer. *Annu. Rev. Cell Dev. Biol.* **2006**, *22*, 287–309.

(23) Petrie, R. J.; Doyle, A. D.; Yamada, K. M. Random versus Directionally Persistent Cell Migration. *Nat. Rev. Mol. Cell Biol.* **2009**, *10*, 538–549.

(24) Worthylake, R. a; Burridge, K. RhoA and ROCK Promote Migration by Limiting Membrane Protrusions. *J. Biol. Chem.* **2003**, *278*, 13578–13584.

(25) Pankov, R.; Endo, Y.; Even-Ram, S.; Araki, M.; Clark, K.; Cukierman, E.; Matsumoto, K.; Yamada, K. M. A Rac Switch Regulates Random versus Directionally Persistent Cell Migration. *J. Cell Biol.* **2005**, *170*, 793–802.

(26) Koons, B.; Sharma, P.; Ye, Z.; Mukherjee, A.; Lee, M. H.; Wirtz, D.; Behkam, B.; Nain, A. S. Cancer Protrusions on a Tightrope: Nanofiber Curvature Contrast Quantitates Single Protrusion Dynamics.

ACS Nano **2017**, *11*.
(27) Nain, A. S.; Sitti, M.; Jacobson, A.; Kowalewski, T.; Amon, C. Dry Spinning Based Spinneret Based Tunable Engineered Parameters (STEP) Technique for Controlled and Aligned Deposition of Polymeric Nanofibers. *Macromol. Rapid Commun.* **2009**, *30*.
(28) Wang, J.; Nain, A. S. Suspended Micro/Nanofiber Hierarchical Biological Scaffolds Fabricated Using Non-Electrospinning STEP Technique. *Langmuir* **2014**, *30*, 13641–13649.
(29) Nain, A. S.; Phillippi, J. a; Sitti, M.; Mackrell, J.; Campbell, P. G.; Amon, C. Control of Cell Behavior by Aligned Micro/Nanofibrous Biomaterial Scaffolds Fabricated by Spinneret-Based Tunable Engineered Parameters (STEP) Technique. *Small* **2008**, *4*, 1153–1159.
(30) Sheets, K.; Wang, J.; Zhao, W.; Kapania, R.; Nain, A. S. Nanonet Force Microscopy for Measuring Cell Forces. *Biophys. J.* **2016**, *111*, 197–207.
(31) Hall, A.; Chan, P.; Sheets, K.; Apperson, M.; Delaughter, C.; Gleason, T. G.; Phillippi, J. A.; Nain, A. Nanonet Force Microscopy for Measuring Forces in Single Smooth Muscle Cells of the Human Aorta. *Mol. Biol. Cell* **2017**, *28*, 1894–1900.
(32) Terrier, C. G.; Monzo, P.; Zhu, J.; Long, H.; Venkatraman, L.; Zhou, Y.; Wang, P.; Chew, S. Y.; Mogilner, A.; Ladoux, B.; *et al.* Protrusive Waves Guide 3D Cell Migration along Nanofibers. **2015**, *211*.
(33) Giannone, G.; Dubin-Thaler, B. J.; Rossier, O.; Cai, Y.; Chaga, O.; Jiang, G.; Beaver, W.; D??bereiner, H. G.; Freund, Y.; Borisy, G.; *et al.* Lamellipodial Actin Mechanically Links Myosin Activity with Adhesion-Site Formation. *Cell* **2007**, *128*, 561–575.
(34) Pontes, B.; Monzo, P.; Gole, L.; Le Roux, A.-L.; Kosmalska, A. J.; Tam, Z. Y.; Luo, W.; Kan, S.; Viasnoff, V.; Roca-Cusachs, P.; *et al.* Membrane Tension Controls Adhesion Positioning at the Leading Edge of Cells. *J. Cell Biol.* **2017**, *216*, 2959–2977.
(35) Zidovska, A.; Sackmann, E. On the Mechanical Stabilization of Filopodia. *Biophys. J.* **2011**, *100*, 1428–1437.
(36) Tamada, A.; Kawase, S.; Murakami, F.; Kamiguchi, H. Autonomous Right-Screw Rotation of Growth Cone Filopodia Drives Neurite Turning. *J. Cell Biol.* **2010**, *188*, 429–441.
(37) Albrecht-Buehler, G. Filopodia of Spreading 3T3 Cells: Do They Have a Substrate-Exploring Function? *J. Cell Biol.* **1976**, *69*, 275–286.
(38) Bornschlögl, T. How Filopodia Pull: What We Know about the Mechanics and Dynamics of Filopodia. *Cytoskeleton* **2013**, *70*, 590–603.
(39) Strohmeyer, N.; Bharadwaj, M.; Costell, M.; Fässler, R.; Müller, D. J. Fibronectin-Bound A5β1 Integrins Sense Load and Signal to Reinforce Adhesion in Less than a Second. *Nat. Mater.* **2017**, *16*, 1262–1270.
(40) Saarikangas, J.; Zhao, H.; Pykäläinen, A.; Laurinmäki, P.; Mattila, P. K.; Kinnunen, P. K. J.; Butcher, S. J.; Lappalainen, P. Molecular Mechanisms of Membrane Deformation by I-BAR Domain Proteins. *Curr. Biol.* **2009**, *19*, 95–107.
(41) Mattila, P. K.; Lappalainen, P. Filopodia: Molecular Architecture and Cellular Functions. *Nat. Rev. Mol. Cell Biol.* **2008**, *9*, 446–454.
(42) Mogilner, A.; Rubinstein, B. The Physics of Filopodial Protrusion. *Biophys. J.* **2005**, *89*, 782–795.
(43) Tomasello, M.; Kirby, S.; Polich, L.; Senghas, R. J.; Wanner, E.; Gleitman, L. R.; Morford, J. P.; Coppola, M.; Kegl, J.; Senghas, A.; *et al.* Two Distinct Actin Networks Drive the Protrusion Of. *Science (80-.).* **2004**, *305*, 1782–1787.
(44) Mongiu, A. K.; Weitzke, E. L.; Chaga, O. Y.; Borisy, G. G. Kinetic-Structural Analysis of Neuronal Growth Cone Veil Motility. *J. Cell Sci.* **2007**, *120*, 1113–1125.
(45) Guillou, H.; Depraz-Depland, A.; Planus, E.; Vianay, B.; Chaussy, J.; Grichine, A.; Albigès-Rizo, C.; Block, M. R. Lamellipodia Nucleation by Filopodia Depends on Integrin Occupancy and Downstream Rac1 Signaling. *Exp. Cell Res.* **2008**, *314*, 478–488.
(46) Hodor, P. G.; Illies, M. R.; Broadley, S.; Ettensohn, C. A. Cell-Substrate Interactions during Sea Urchin Gastrulation: Migrating Primary Mesenchyme Cells Interact with and Align Extracellular Matrix Fibers That Contain ECM3, a Molecule with NG2-like and Multiple Calcium-Binding Domains. *Dev. Biol.* **2000**, *222*, 181–194.
(47) Wyckoff, J. B.; Pinner, S. E.; Gschmeissner, S.; Condeelis, J. S.; Sahai, E. ROCK- and Myosin-Dependent Matrix Deformation Enables Protease-Independent Tumor-Cell Invasion In Vivo. *Curr. Biol.* **2006**, *16*, 1515–1523.
(48) Bridgman, P. C.; Dailey, M. E. The Organization of Myosin and Actin in Rapid Frozen Nerve Growth

Cones. *J. Cell Biol.* **1989**, *108*, 95–109.
(49) Beningo, K. A.; Wang, Y. L. Flexible Substrata for the Detection of Cellular Traction Forces. *Trends Cell Biol.* **2002**, *12*, 79–84.
(50) Steinwachs, J.; Metzner, C.; Skodzek, K.; Lang, N.; Thievessen, I.; Mark, C.; Münster, S.; Aifantis, K. E.; Fabry, B. Three-Dimensional Force Microscopy of Cells in Biopolymer Networks. *Nat. Methods* **2016**, *13*, 171–176.
(51) Cesa, C. M.; Kirchgessner, N.; Mayer, D.; Schwarz, U. S.; Hoffmann, B.; Merkel, R. Micropatterned Silicone Elastomer Substrates for High Resolution Analysis of Cellular Force Patterns. *Rev. Sci. Instrum.* **2007**, *78*, 034301.
(52) Doyle, A. D.; Wang, F. W.; Matsumoto, K.; Yamada, K. M. One-Dimensional Topography Underlies Three-Dimensional Fibrillar Cell Migration. *J. Cell Biol.* **2009**, *184*, 481–490.
(53) Harley, B. a C.; Kim, H.-D.; Zaman, M. H.; Yannas, I. V; Lauffenburger, D. a; Gibson, L. J. Microarchitecture of Three-Dimensional Scaffolds Influences Cell Migration Behavior via Junction Interactions. *Biophys. J.* **2008**, *95*, 4013–4024.

TABLE OF CONTENT (TOC)

Anisotropically stretched cells form lateral nano-twines (yellow arrow) anywhere along their length. 3D freely-swinging twines engage with neighboring fibers in few seconds, which acts as a catalyst for formation of twine-bridges comprised of at least two individual twines (red arrow). Perpendicular lateral protrusions (PLPs) oriented perpendicular to cell body migration direction (green arrow) mature into broad structures (blue arrow) capable of exerting tens of nanonewton forces that allow cells to stretch laterally.

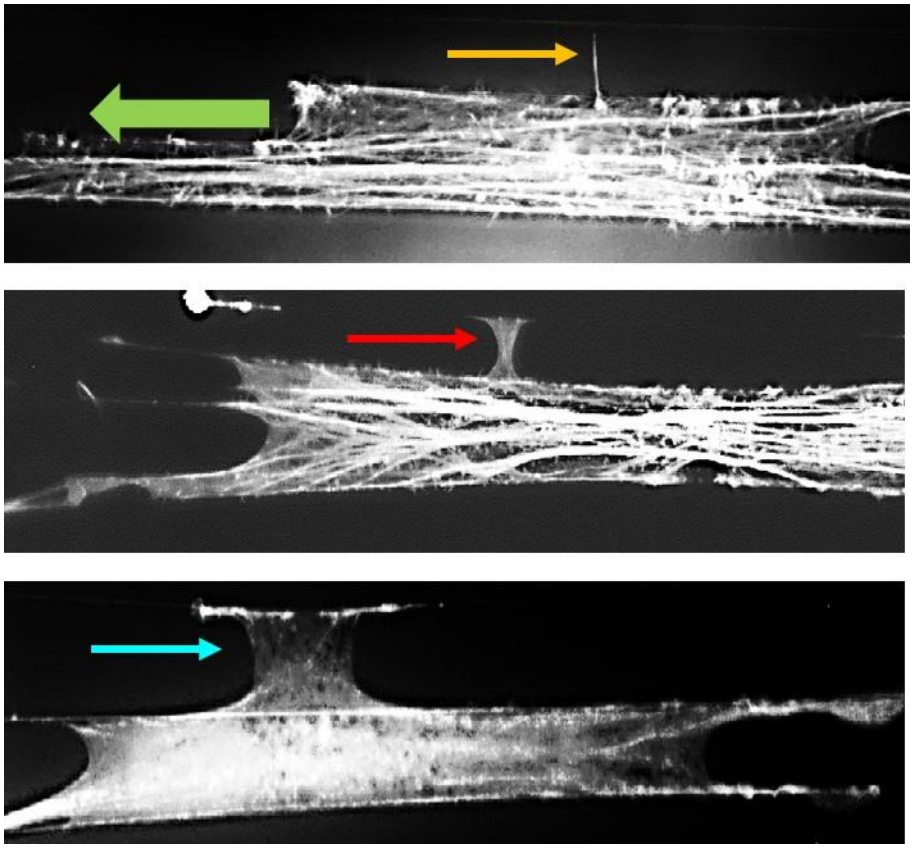

MOVIES

Movie S1. PLPs in mouse myoblast C2C12: Lateral protrusion (shown by arrows) that develops into lamellipodial resembling structure to spread on neighboring fiber. Time shown on top left in hours:minutes:seconds

Movie S2: PLPs in mouse fibroblast 3T3: Lateral protrusion (shown by arrows) that develops into lamellipodial resembling structure to spread on neighboring fiber. Time shown on top left in minutes:seconds

Movie 3.PLPs in mouse embryonic fibroblast (MEF): Lateral protrusion (shown by arrows) that develops into lamellipodial resembling structure to spread on neighboring fiber. Time shown on top left in hours:minutes:seconds

Movie 4. PLPs in Human cervical tumor HeLa: Lateral protrusion (shown by arrows) that develops into lamellipodial resembling structure to spread on neighboring fiber. Time shown on top left in hours:minutes:seconds

Movie 5: PLPss in primary human mesenchymal stem cells (hMSC): Lateral protrusion (shown by arrows) that develops into lamellipodial resembling structure to spread on neighboring fiber. Time shown on top left in hours:minutes:seconds

Movie 6. Actin waves along cell body: Membrane ruffles spiral as actin wave about fiber axis. Time shown on top left in hours:minutes:seconds

Movie 7. Lateral *twines* form through membrane ruffles: Membrane ruffles extending from cell body stratify into denser structures or *twines.* Time shown on top left in seconds:thousandths

Movie 8. *Twine* engagement with neighboring fibers: *Twine* engagement to neighboring fiber occurs in 1-2 s. Time shown on top left in seconds:thousandths

Movie 9. Establishment of *twine-bridges:* Growth of actin lamellum at the base of primary *twine* followed by formation of secondary *twine* and establishment of primary-secondary *twine-bridge* that facilitates the growth of actin lamellum over long distances without branching. Time shown on top left in seconds:thousandths

Movie 10. Ruffle attaching to neighboring fiber: Actin ruffles can attach directly to neighboring parallel fibers of low interfiber spacing without going through the steps of PLP formation.

Movie 11. Thick *twines* attaching to neighboring fibers: Thick twines can attach directly to neighboring fibers of low interfiber spacing without going through the steps of PLP formation.

Movie 12. Attachment angle change of twine to form PLP: Twines angled to parent cell body become PLPs as cell body moves thus changing the angle of attachment. Time shown in minutes.

Movie 13. Live f-actin stress fiber imaging: A cell attached to five fibers is imaged for one hour to measure transient changes in f-actin stress fiber angles. The tracked stress fibers are shown by triangles next to them.

<u>Movie 14.</u> Cell migration on a 9-fiber system: Anisotropic cell attached to 9-fiber system and forming lateral protrusions at attachments in top and bottom 3-fiber sets. Time shown on top left in seconds